Transportation Research Part C 73 (2016) 219–238

Contents lists available at ScienceDirect

Transportation Research Part C

journal homepage: www.elsevier.com/locate/trc

Integrated signal optimization and non-traditional lane assignment for urban freeway off-ramp congestion mitigation

Jing Zhao [a], Yue Liu [b,*]

[a] University of Shanghai for Science and Technology, 516 Jungong Road, Shanghai, PR China
[b] Department of Civil and Environmental Engineering, University of Wisconsin at Milwaukee, P.O. Box 784, Milwaukee, WI, United States

ARTICLE INFO

Article history:
Received 22 February 2016
Received in revised form 23 September 2016
Accepted 6 November 2016
Available online 14 November 2016

Keywords:
Urban freeway
Off-ramps
Non-traditional lane assignment
Integrated design
Capacity
Signal optimization

ABSTRACT

Exiting flow from urban freeway off-ramps coupled with limited capacity and traffic weaving at the downstream intersections creates major bottlenecks in urban road network. This paper presents an integrated design model for non-traditional lane assignment and signal optimization at the off-ramp, its downstream intersection, and their connecting segment with the objective to mitigate or eliminate traffic weaving and to maximize the section's overall capacity. A mixed-integer non-linear program model is formulated to capture real-world operational constraints regarding the non-traditional lane assignment, special phasing treatment and signal timing. The mathematical model is linearized and solved by the standard branch-and-bound technique. Extensive numerical analysis and case study results validate the effectiveness of the proposed integrated model and demonstrate its promising application at locations where the upstream freeway off-ramp is located at the middle of the road cross section and the space between the stop line and off-ramp is limited.

1. Introduction

Traffic on urban freeway off-ramps often experiences difficulty in exiting due to its competition with traffic from surface streets. Using Fig. 1 as an example, when the space between the off-ramp and the downstream intersection is limited, queue at the downstream intersection during the red phase may easily prevent the off-ramp exiting traffic from merging into their target approach lanes. The resulting queue on the off-ramp then generates a spillover onto the mainstream of the urban freeways, resulting in freeway mobility loss and traffic safety problems (Cassidy et al., 2002; Cheu et al., 1998; Daganzo et al., 1999; Jin et al., 2002; Newell, 1999). On the other hand, poor utilization of the downstream intersection capacity may occur due to the fact that insufficient weaving space between freeway and surface street traffic induces extra delays and prevents vehicles from reaching the downstream stop line during the green time (TRB, 2010). Due to the aforementioned problems, off-ramps, the downstream signalized intersections, and their connecting segments often constitute the major bottlenecks in the urban road network.

To mitigate traffic congestion at those bottlenecks, transportation researchers have been investigating and implementing a variety of strategies. In review of literature, these strategies mainly fall into the following two categories: demand or access management strategies and traffic management strategies (Munoz and Daganzo, 2002; Rudjanakanoknad, 2012; Spiliopoulou et al., 2014).

* Corresponding author.
E-mail addresses: jing_zhao_traffic@163.com (J. Zhao), liu28@uwm.edu (Y. Liu).

http://dx.doi.org/10.1016/j.trc.2016.11.003
0968-090X/

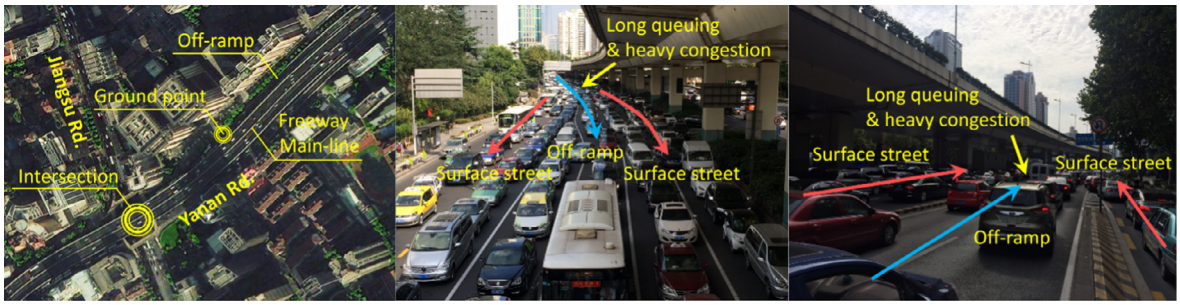

(a) Aerial view (b) View from the intersection (c) View from the end of the off-ramp

Fig. 1. Example of the complex operation condition in real world (Jiangsu Rd. and Yanan Rd. in Shanghai, China).

Demand or access management strategies improve the performance of the off-ramp areas by denying access to the preferred off-ramp once the off-ramp queue has emerged onto the freeway, or by guiding traffic to upstream ramps by variable message signs (Daganzo et al., 2002). The system optimum dynamic traffic assignment is studied at a network level (Muñoza and Laval, 2006). Since it may represent a high penalty for detoured vehicles, especially when the nearby off-ramps are far away, application of such strategies may be limited only to the special events such as those associated with large sporting events and emergency conditions such as evacuation (Liu et al., 2011, 2013). In addition, traffic demand of the freeway could also be reduced by pricing (Shen and Zhang, 2009). Although there are equity issues, it may be considered on major bottlenecks in big cities. Moreover, the road pricing strategies could be flexibly combined with other management methods (Sheu and Yang, 2008; Zhong et al., 2014).

Traffic demand diversion strategies in surface streets have also been adopted to reduce off-ramp traffic demand by detouring a certain fraction of the side road flow through underutilized and nearby parallel roads (Günther et al., 2012). There are two alternatives: detouring the flow on the side road to the local network and detouring the flow on the cross street to the local network. The former could eliminate the weaving movement upstream of the intersection, while the latter could reduce the degree of saturation of the intersection. However, these strategies would certainly cause extra driving distances and may shift traffic congestion to somewhere else in the network.

Different from demand or access management strategies, traffic management strategies mitigate off-ramp and adjacent intersection congestion by enhancing their capacities or utilization of capacities. For examples, reassigning lane usage at the freeway diverge gore area is used to mitigate the congestion caused by the insufficiency of the off-ramp capacity (Daganzo et al., 2002; Hagen et al., 2006).

At the surface street side, off-ramp congestion is mostly caused by traffic weaving or insufficient capacity of the downstream intersections (Denney et al., 2009; Lu et al., 2010; Tian et al., 2007). A number of models have been proposed to optimize the signal timing of the downstream intersection. In these models, queue detectors are installed at the upstream end of the off-ramp to prevent queue spillback onto the freeway. However, if the objective only focuses on managing traffic operation from the perspective of optimizing freeway traffic flow, the normal signal operations on the surface street will be disrupted significantly (Tian et al., 2002). In view of such deficiencies, integrated signal control models and strategies have been developed with the objective to minimize the total delay for off-ramps and their connected surface streets (Li et al., 2009; Lim et al., 2011; Mirchandani and Head, 2001; Tian and Wu, 2012; Yang et al., 2014). These signal timing strategies are useful to relieve congestion due to the fluctuation of freeway traffic and stochastic arrival pattern at the off-ramp. However, when the downstream intersection is oversaturated due to high traffic demand, lane markings of the intersection should be reorganized to further improve the intersection capacity (Hagen et al., 2006). To this regard, researchers have found that the use of dual right-turn lanes may facilitate weaving for right-turning vehicles from the off-ramp and increase the capacity of the intersection in proximity to off-ramps which are characterized by higher turning volumes (Chen et al., 2014; Yi et al., 2012). However, in most of previous studies optimizing intersection channelization to reduce traffic weaving between freeway and surface street is neglected and reorganization of the weaving segment between the intersection and off-ramp has not been considered. Additionally, very limited efforts have been made for integrated geometric layout and signal timing optimization for the off-ramp and its proximity surface street section.

In this paper, we develop an integrated design model for non-traditional lane assignment and signal optimization at the off-ramp, its downstream intersection, and their connecting segment with the objective to mitigate or eliminate traffic weaving and to maximize the section's overall capacity. Please note there are several types of ramp-street connection designs, such as the off-ramp connecting with a surface street, directly connecting with the intersection, and connecting with a local arterial with multiple adjacent intersections (Yang et al., 2015). The method proposed in this paper is mainly used on the condition that the off-ramp is connected with a surface street with an intersection at the downstream.

The idea of an integrated design is not new. Lam et al. (1997) combines the design of lane markings and signal timings and pointed out its potential benefits in improving intersection performance. To optimize these design variables in a unified framework, the lane-based optimization method was developed (Wong and Wong, 2002, 2003b). The modelling method defines all key design variables on a lane-basis. This makes it easier to express the set of constraints as linear equations, thus

ensuring the feasibility of the solution algorithm for the optimization model. These years, the lane-based modelling method continues to develop and expands the application scope. At the intersection level, Wong and Wong (2003a) firstly developed some lane-based models to optimize the lane markings of the approaches and the signal timings simultaneously in a unified framework. According to the difference in the optimization objective, they can be divided into three sub-models: capacity maximization, cycle length minimization, and delay minimizing. Wong et al. (2006) extended this method to deal with the problem that the traffic demand varies in various periods, e.g. the morning peak, off peak and evening peak periods. It is assumed that numbers of approach and exit lanes in different arms are fixed in these models. To remedy this deficiency, Wong and Heydecker (2011) further included the lane arrangement between the approach and exit into the original lane-based optimization model to achieve better intersection capacity. The lane-based modelling method also helped to improve the operational efficiency of some unconventional intersections, in which some new modelling problem should be solved. E. g., Zhao et al. (2013) presented an innovative intersection design which is known as the exit lanes for left-turn (EFL) intersection design. A lane-based optimization model for EFL control was formulated to simultaneously optimize the lane assignment of the intersection, the length of the mixed-usage-area, and the timing of both the main signal and the pre-signal. Yan et al. (2014) established a lane-based optimization model for the tandem sorting strategy to coordinate the pre-signals on all arms and the intersection signal, in which all through, left- and right-turning movements on all arms were explicitly taken into consideration. Ma et al. (2014) developed a lane-based model for the exclusive bus lanes design at isolated intersections with the consideration of two traffic modes, passenger cars and buses. The optimization of lane markings, exclusive bus lanes, and passive bus priority signal settings for isolated intersections have been combined in a unified framework. Person capacity maximization has been adopted as a criterion for the integrated optimization model. Zhao et al. (2014a) proposed a lane-based optimization model for the median U-turn intersection and formulated a multi objective mixed-integer nonlinear programming problem to optimize the intersection design types, the layout of the intersection, and the signal timings simultaneously. Sun et al. (2015) proposed a simplified continuous flow intersection (called CFI-Lite) design, which uses the existing upstream intersection, instead of newly constructed sub-intersection, to allocate left-turn traffic to displaced left-turn lane. The research also formulates a lane-based optimization model to seek for Pareto capacity improvements. Lee et al. (2015) developed a method for the real-time estimation of lane-based queue lengths. He et al. (2016) established a lane-based optimization model for grade separation at signalized intersections, in which the grade-separated lanes (e.g. tunnels), lane markings, and signal timing settings are integrated. Moreover, the lane-based modelling method also extended to the arterial and network level, researchers analyzed the interaction of the signalized intersections, and combined lane channelization, signal settings, network routing decisions, reversible lane settings, turning restrictions, etc. (Cantarella et al., 2006; Mahalel and David, 2014; Zhao et al., 2014b).

All of the aforementioned methods take the constraints that the allocation of the left-turn, through, and right-turn lanes should be ordered from left to right (under the condition that vehicles drive on the right side of the road) to eliminate potential internal-cross conflicts within an arm, see Fig. 2 for an example. In this paper, this traditional channelization restriction was relaxed. Some special lane assignment schemes (SLA) are proposed to mitigate or eliminate traffic weaving (see Fig. 3 for an example of non-traditional layout of left-turn and through lanes with eliminated weaving between off-ramp left-turn and the surface street through movement). To ensure the operational safety, special signal phases at the downstream intersection should be designed accordingly, which may cause negative effect on the operation efficiency of the intersection, since some well-designed phase plan, such as the dual-ring phases, could not be used. It becomes a very complex interaction and one needs to address the trade-off.

This paper aims to discuss the following critical operation issues: (1) how to optimize the design of SLA integrated with the signal timing of the intersection? and (2) what is the performance and application domain of SLA in comparison with the conventional design? The impact of the off-ramp on the downstream intersection saturation flow rates will be quantified and special signal phasing schemes will be developed and coordinated with the non-traditional lane assignment in a unified optimization framework. The performance of the integrated design model will be evaluated using extensive numerical tests and case studies. Conditions for best application of the proposed model will also be examined via sensitivity analyses.

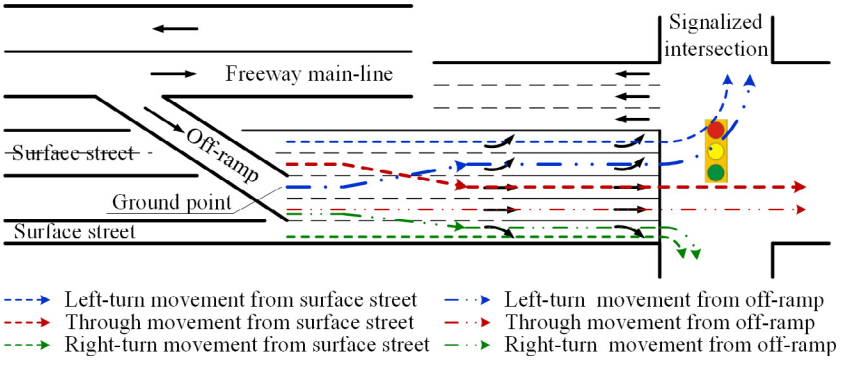

Fig. 2. A traditional lane assignment example.

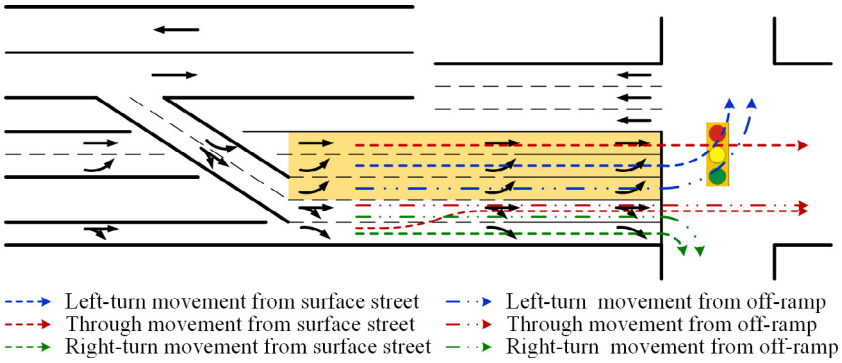

Fig. 3. A non-traditional lane assignment example.

The rest of this paper is organized as follows. The non-traditional lane assignment and special signal control concept are illustrated in Section 2. Section 3 presents the mixed-integer-linear-program optimization model for integrated lane assignment and signal design. Section 4 performs extensive numerical and simulation analyses to validate the effectiveness of the proposed model and to identify its best application domain. Conclusions and recommendations are given at the end of the paper.

2. The operational concept

The basic idea of the non-traditional lane assignment strategy is to allow internal conflicts among lanes within an approach, which include six typical types, as illustrated in Table 1.

Considering the internal conflicts between traffic movements due to non-traditional lane assignment, special signal phases at the downstream intersection should be designed. Without loss of generality, assuming that the off-ramp is located at the west leg of the intersection, then the phasing sequence corresponding to each of the six conflicting movement types can be represented with the precedence graphs (Head et al., 2007) in Fig. 4 (only the East-West direction is shown, the South-North direction could use the dual-ring signal phase), in which the solid arcs indicate the activity (duration of green of a movement), the nodes indicate the end of the prior-activity and start of the back closely activity (start of green), and the dot arcs represent precedence relationships with time constraints.

3. The integrated design model

Grounded operational concept in Section 2, an optimization model integrating the selection of non-traditional lane assignment strategies, setting of lane markings, and signal optimization is developed.

Table 1
Six typical non-traditional lane assignment design types.

No.	Design type	Description	Illustration
1	LT-TH conflict	Left-turn lanes are located at the right side of through lanes	
2	TH-RT conflict	Through lanes are located at the right side of right-turn lanes	
3	LT-TH + LT-RT conflict	Left-turn lanes are located at the right side of through and right-turn lanes	
4	LT-TH + TH-RT conflict	Part of through lanes are located at the left side of left-turn lanes and others are located at the right side of right-turn lanes	
5	LT-RT + TH-RT conflict	Right-turn lanes are located at the left side of left-turn and through lanes	
6	LT-TH-RT conflict	Part of through lanes are located at the left side of left -turn lanes, other through lanes are located at the right side of right-turn lanes, and left-turn lanes are located at the right side of right-turn lanes	

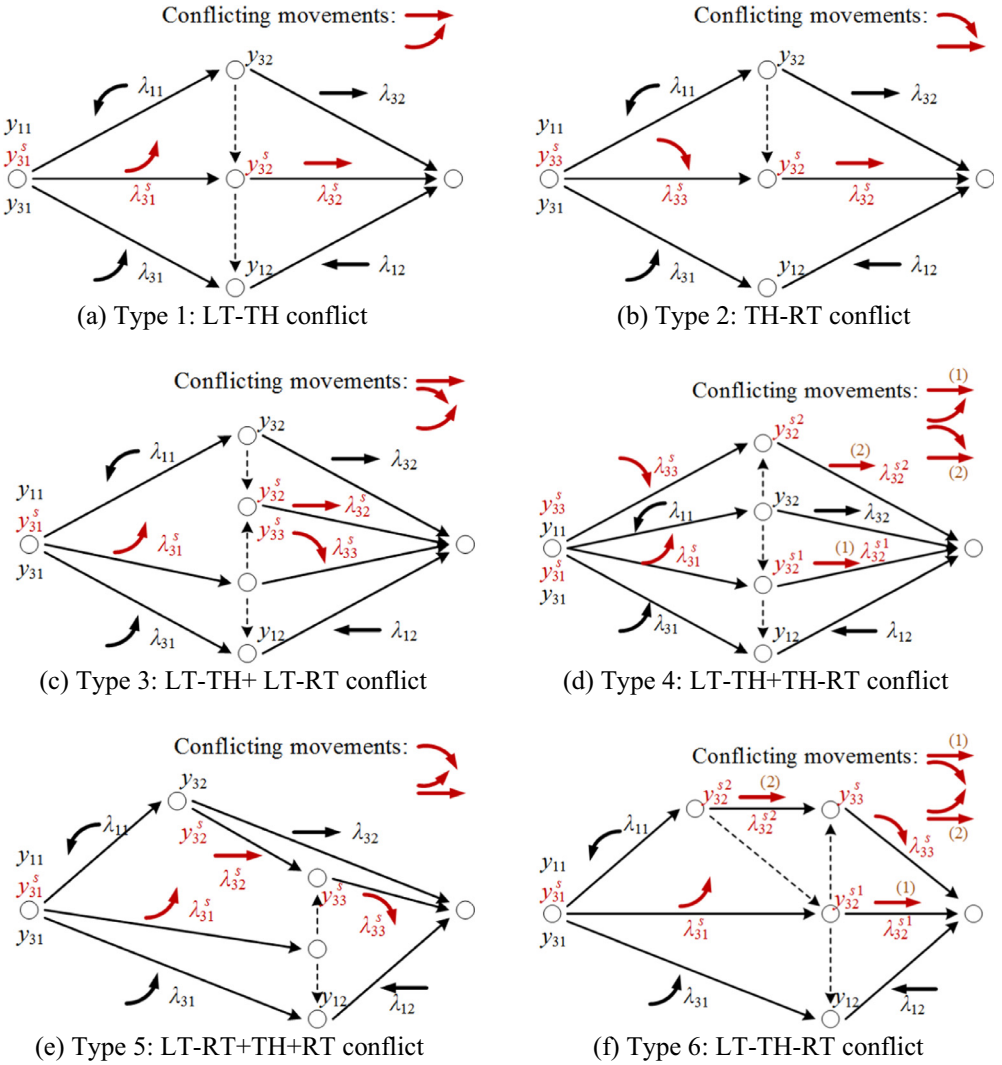

Fig. 4. Representation of signal phasing with precedence graphs for six non-traditional lane assignment design types Note: y_{iw} is the start of green for movement w on leg i for normal movements; y_{iw}^{s}, y_{iw}^{s1}, y_{iw}^{s2} are start of green for movement w on leg i for conflicting movements; λ_{iw} is the green time ratio for movement w on leg i for normal movements; λ_{iw}^{s}, λ_{iw}^{s1}, λ_{iw}^{s2} is the green time ratio for movement w on leg i for conflicting movements; i is the index of legs, $i = 1$ for east leg, $i = 2$ for south leg, $i = 3$ for west leg, and $i = 4$ for north leg; w is turning movements, $w = 1$ for left-turn, $w = 2$ for through movement, and $w = 3$ for right-turn.

3.1. Notations

To facilitate the model presentation, notations used hereafter are summarized in Table 2. They are divided into three categories: parameters (model inputs), decision variables (model outputs), and auxiliary variables. Fig. 5 illustrates the layout of key geometric parameters.

3.2. Objective function

The proposed model aims to maximize the reserve capacity of the analysis section including the off-ramp downstream intersection and their connecting segment. Adopting the commonly used assumption that the turn proportions would remain constant (Gallivan and Heydecker, 1988), maximizing the reserve capacity is equivalent to maximizing the common flow multiplier. A value of $\mu < 1$ indicates that the analysis section is overloaded by $100(1-\mu)$ percent, and a value of $\mu > 1$ indicates a reserve capacity of $100(\mu-1)$ percent.

$$max \quad \mu \tag{1}$$

Table 2
Notation of key model parameters and variables.

Sets and parameters	
$\mathcal{L}$	Set of legs
$i \in \mathcal{L}$	Index of legs, $i = 1$ for east leg, $i = 2$ for south leg, $i = 3$ for west leg, and $i = 4$ for north leg, as illustrated in Fig. 5
$\mathcal{S}$	Set of sections in a leg
$r \in \mathcal{S}$	Index of section in a leg, $r = 1$ for approach, $r = 2$ for road segment including the off-ramp and surface street
$\mathcal{T}$	Set of turning movements
$w \in \mathcal{T}$	Index of turning movements, $w = 1$ for left-turn, $w = 2$ for through movement, and $w = 3$ for right-turn, as illustrated in Fig. 5
k	Index of lanes, numbering from the left most lane, as illustrated in Fig. 5
Q^l_{iw}	Volume of movement w on leg i at the intersection (veh/h)
Q^s_{iw}	Volume of movement w on leg i from surface street (veh/h), as illustrated in Fig. 5
Q^f_{iw}	Volume of movement w on leg i from freeway off-ramp (veh/h), as illustrated in Fig. 5
n_{ir}	Number of lanes on leg i at section r
n^e_{iw}	The number of lanes at the corresponding receiving leg of movement w on leg i
n_{il}	Number of lanes from which a weaving maneuver may be made with one or no lane changes
l_i	Distance between the stop line and freeway off-ramp ground point on leg i (m), as illustrated in Fig. 5
l_{iw}	Length of the weaving segment (m), as illustrated in Fig. 5
p^s_{i2k}	A binary variable indicating whether the lane k on leg i at the road segment is from surface street (1-yes, 0-no), as illustrated in Fig. 5
p^f_{i2k}	A binary variable indicating whether the lane k on leg i at the road segment is from freeway off-ramp (1-yes, 0-no), as illustrated in Fig. 5
C_{min}, C_{max}	Minimum and maximum cycle length (s)
I	Clearance time for a pair of conflicting traffic movements (s)
s^o_{ik}	Saturation flow rate on lane k on leg i (veh/h)
c_f	Capacity of a basic segment under ideal conditions, per lane (veh/h/ln)
h_q	Average space headway for queuing vehicles (m)
d_{max}	Maximum acceptable degree of the saturation
M	An arbitrarily large positive constant number
Decision variables	
μ	Common flow multiplier of the intersection
q_{irkw}	Volume of movement w on leg i at section r using lane k (veh/h)
$q_{iw(2k,1k')}$	Volume of movement w from lane k at the road segment to lane k' at the intersection on leg i (veh/h)
$\eta_{iw(2k,1k')}$	A binary variable indicating whether the movement w from lane k at the road segment to lane k' at the intersection is a weaving movement
x_{irkw}	A binary variable indicating the permission of movement w on lane k on leg i at section r (1-permitted, 0-prohibited)
ξ	Reciprocal of cycle length (1/s)
y_{iw}	Start of green for movement w on leg i for normal movements
y^s_{iw}, y^{s1}_{iw}, y^{s2}_{iw}	Start of green for movement w on leg i for conflicting movements
λ_{iw}	Green time ratio for movement w on leg i for normal movements
λ^s_{iw}, λ^{s1}_{iw}, λ^{s2}_{iw}	Green time ratio for movement w on leg i for conflicting movements
Auxiliary variables	
c_{ik}	Capacity of the lane k on leg i at the intersection (veh/h)
$q^u_{iw(2k,1k')}$	Weaving volume of movement w from lane k at the road segment to lane k' at the intersection on leg i (veh/h)
V_{iR}	Weaving volume ratio
β_{ip}	A binary variable indicating the selection of non-traditional lane assignment design type p on leg i (1-selected, 0-not selected)
$\delta_{iww'}$	A binary variable indicating the existence of internal conflicts between movement w and movement w' on leg i (1-yes, 0-no), δ_{i12} for left-turn and through movement (LT-TH) conflict, δ_{i13} for left-turn and right-turn (LT-RT) conflict, δ_{i23} for through movement and right-turn (TH + RT) conflict
δ_{irk}	A binary variable indicating whether the lane k on leg i at section r is a special lane (1-yes, 0-no)
n^u_i	Number of lanes in the weaving segment on leg i
C	Cycle length (s)
Y_{ik}	Start of green on lane k on leg i at the intersection
Λ_{ik}	Green time ratio for lane k on leg i at the intersection
T^o_{ik}	Portion of the green time ratio during which the vehicles discharge under saturation flow rate
T^u_{ik}	Portion of the green time ratio during which the vehicles discharge as weaving flow
T^q_{ik}	The time queue cleared
T^{b1}_{ik}	Start time of blockage for the adjacent lane of lane k on leg i
T^{b2}_{ik}	End time of blockage for the adjacent lane of lane k on leg i
α^{b1}_{ik1}, α^{b1}_{ik2}, α^{b2}_{ik1}, α^{b2}_{ik2}	Loop integer variables to ensure that T^{b1}_{ik} and T^{b2}_{ik} will be within a fraction between $Y_{ik} + \Lambda_{ik} - 1$ and $Y_{ik} + \Lambda_{ik}$
s^u_{ik}	Weaving flow rate on lane k on leg i (veh/h)

3.3. Constraints

3.3.1. Lane assignment constraints

For lane assignment, the permission of movement w on each lane on each leg at the intersection and road segment, x_{irkw}, is the key decision variable and is dependent on the following modules (see Fig. 6): (1) selection of design types, β_{ip}; (2) identification of internal conflicts, $\delta_{iww'}$; (3) determination of lanes with non-traditional lane-use, δ_{irk}; and (4) other general layout constraints.

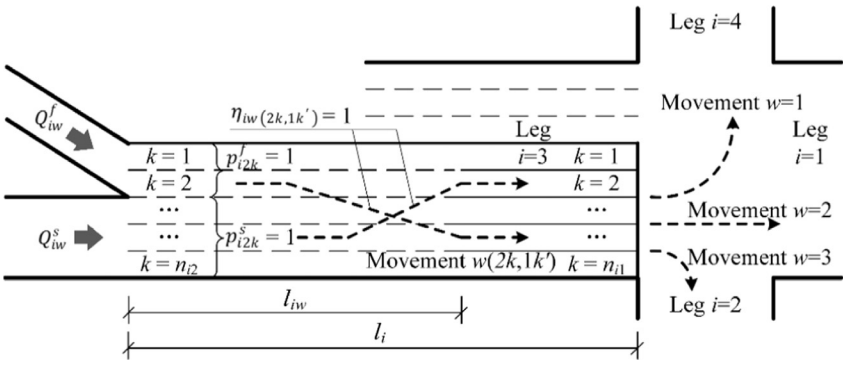

Fig. 5. Schematic layout indicating the geometric parameters.

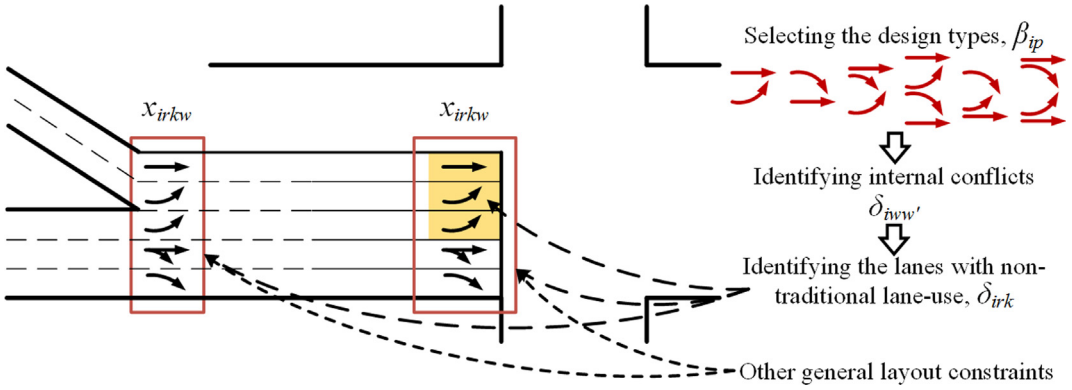

Fig. 6. Key components of lane assignment constraints.

(1) The variable used to select non-traditional lane assignment design type, β_{ip}, could be determined by judging the existence of the left-turn and through movement (LT-TH) conflict (δ_{i12}), the left-turn and right-turn (LT-RT) conflict (δ_{i13}), and the through movement and right-turn (TH + RT) conflict (δ_{i23}). E.g., as shown in constraint (2), the non-traditional lane assignment design type 1 will be selected ($\beta_{i1} = 1$) when only the LT-TH conflict exists ($\delta_{i12} = 1$, $\delta_{i13} = \delta_{i23} = 0$). Other design types could be determined similarly by constraint (3)–(7).

$$\beta_{i1} = \delta_{i12}(1-\delta_{i13})(1-\delta_{i23}), \qquad \forall i \in \mathcal{L} \tag{2}$$

$$\beta_{i2} = (1-\delta_{i12})(1-\delta_{i13})\delta_{i23}, \qquad \forall i \in \mathcal{L} \tag{3}$$

$$\beta_{i3} = \delta_{i12}\delta_{i13}(1-\delta_{i23}), \qquad \forall i \in \mathcal{L} \tag{4}$$

$$\beta_{i4} = \delta_{i12}(1-\delta_{i13})\delta_{i23}, \qquad \forall i \in \mathcal{L} \tag{5}$$

$$\beta_{i5} = (1-\delta_{i12})\delta_{i13}\delta_{i23}, \qquad \forall i \in \mathcal{L} \tag{6}$$

$$\beta_{i6} = \delta_{i12}\delta_{i13}\delta_{i23}, \qquad \forall i \in \mathcal{L} \tag{7}$$

(2) Identification of the internal conflicts between movement w and movement w' among lanes within an approach (δ_{i12}, δ_{i13}, and δ_{i23}) could be fulfilled by constraints (8). If any movement w' ($w' > w$) is permitted on lane k' ($k' < k$), the item $\sum_{k=2}^{n_{i1}}\sum_{k'=1}^{k-1}\left\lfloor\frac{x_{i1kw}+x_{i1k'w'}}{2}\right\rfloor$ will be no less than 1. Then, it indicates that the internal conflicts between movement w and movement w' exist ($\delta_{iww'} = 1$). Otherwise, if no movement w' ($w' > w$) is permitted on lane k' ($k' < k$), the item $\sum_{k=2}^{n_{i1}}\sum_{k'=1}^{k-1}\left\lfloor\frac{x_{i1kw}+x_{i1k'w'}}{2}\right\rfloor$ will be equal to 0. Then, it indicates that the internal conflicts between movement w and movement w' does not exist ($\delta_{iww'} = 0$). For example, when the left-turn is permitted on lane k and the through movement is permitted on the left side of lane k (lane k') on leg i at the approach, we have $\left\lfloor\frac{x_{i1k1}+x_{i1k'2}}{2}\right\rfloor = 1$. If any two lanes satisfied

the above situation, according to constraint (8), we have $M \geqslant \delta_{i12} \geqslant \frac{1}{M}$; so $\delta_{i12} = 1$. It indicates that the LT-TH conflict exists on leg i. Otherwise, if none of the two lanes satisfied the above situation, according to constraint (8), we have $0 \geqslant \delta_{i12} \geqslant 0$; so $\delta_{i12} = 0$. It indicates that the LT-TH conflict does not exist on leg i. Similarly, the existence of the LT-RT conflict and the TH + RT conflict could also be identified according to constraint (8).

$$M\sum_{k=2}^{n_{i1}}\sum_{k'=1}^{k-1}\left\lfloor\frac{x_{i1kw}+x_{i1k'w'}}{2}\right\rfloor \geqslant \delta_{iww'} \geqslant \frac{1}{M}\sum_{k=2}^{n_{i1}}\sum_{k'=1}^{k-1}\left\lfloor\frac{x_{i1kw}+x_{i1k'w'}}{2}\right\rfloor, \qquad \forall i \in \mathcal{L}; \quad w \in \mathcal{T} \tag{8}$$

(3) For any traffic lane, constraint (9) could be used to identify whether the lane is a special traffic lane. If any movement w' ($w' > w$) is permitted on lane k' ($k' < k$) or any movement w' ($w' < w$) is permitted on lane k' ($k' > k$), the item $\sum_{w\in\mathcal{T}}\left(\sum_{w'=w+1}^{w+2}\sum_{k'=1}^{k-1}\left\lfloor\frac{x_{i1kw}+x_{i1k'w'}}{2}\right\rfloor + \sum_{w'=w-2}^{w-1}\sum_{k'=k+1}^{n_{i1}}\left\lfloor\frac{x_{i1kw}+x_{i1k'w'}}{2}\right\rfloor\right)$ will be no less than 1. Then, it indicates that the lane k is a special traffic lane ($\delta_{i1k} = 1$). Otherwise, if no movement w' ($w' > w$) is permitted on lane k' ($k' < k$) and no movement w' ($w' < w$) is permitted on lane k' ($k' > k$), the item $\sum_{w\in\mathcal{T}}\left(\sum_{w'=w+1}^{w+2}\sum_{k'=1}^{k-1}\left\lfloor\frac{x_{i1kw}+x_{i1k'w'}}{2}\right\rfloor + \sum_{w'=w-2}^{w-1}\sum_{k'=k+1}^{n_{i1}}\left\lfloor\frac{x_{i1kw}+x_{i1k'w'}}{2}\right\rfloor\right)$ will be equal to 0. Then, it indicates that the lane k is not a special traffic lane ($\delta_{i1k} = 0$).

$$\begin{aligned} &M\sum_{w\in\mathcal{T}}\left(\sum_{w'=w+1}^{w+2}\sum_{k'=1}^{k-1}\left\lfloor\frac{x_{i1kw}+x_{i1k'w'}}{2}\right\rfloor + \sum_{w'=w-2}^{w-1}\sum_{k'=k+1}^{n_{i1}}\left\lfloor\frac{x_{i1kw}+x_{i1k'w'}}{2}\right\rfloor\right) \geqslant \delta_{i1k} \\ &\geqslant \frac{1}{M}\sum_{w\in\mathcal{T}}\left(\sum_{w'=w+1}^{w+2}\sum_{k'=1}^{k-1}\left\lfloor\frac{x_{i1kw}+x_{i1k'w'}}{2}\right\rfloor + \sum_{w'=w-2}^{w-1}\sum_{k'=k+1}^{n_{i1}}\left\lfloor\frac{x_{i1kw}+x_{i1k'w'}}{2}\right\rfloor\right), \qquad \forall i \in \mathcal{L}, \quad k \in \{1,\ldots,n_{i1}\} \end{aligned} \tag{9}$$

(4) Moreover, a traffic lane should permit at least one movement, as shown in constraint (10). Additionally, the number of lanes at the corresponding receiving leg of a movement should be at least as many as the total number of lanes assigned to permit such a movement, in order to prevent the undesirable traffic merging activities. This could be specialized by constraint (11).

$$\sum_{w\in\mathcal{T}} x_{irkw} \geqslant 1, \qquad \forall i \in \mathcal{L}, \quad r \in \mathcal{S}, \quad k \in \{1,\ldots,n_{ir}\} \tag{10}$$

$$n^e_{iw} \geqslant \sum_{k=1}^{n_{i1}} x_{i1kw}, \qquad \forall i \in \mathcal{L}, \quad w \in \mathcal{T} \tag{11}$$

3.3.2. Signal control constraints

According to the precedence graphs in Fig. 4, the signal operational constraints in the proposed model include:

(1) The common cycle length for the intersection to be within the values of C_{min} and C_{max}. According to prior work (Wong and Wong, 2003a,b; Wong and Heydecker, 2011), instead of defining the cycle length directly as the control variable, its reciprocal $\xi = 1/C$, is used to preserve the linearity in the mathematical formulation of signal timing.

$$\frac{1}{C_{min}} \geqslant \xi \geqslant \frac{1}{C_{max}} \tag{12}$$

(2) The phasing plan for normal movements is given by constraints (13)–(19), which is a dual-ring concurrent phasing scheme with assigned movements. For easy discussion, the starts of green for left-turn on east and west legs are equal to 0. For conflicting movements, the start of green and green time ratio should be adjusted according to Fig. 4.

$$y_{i1} = 0, \qquad \forall i \in \{1,3\} \tag{13}$$

$$y_{12} - y_{31} - \lambda_{31} - I\xi = 0 \tag{14}$$

$$y_{32} - y_{11} - \lambda_{11} - I\xi = 0 \tag{15}$$

$$y_{21} = y_{41} = y_{12} + \lambda_{12} + I\xi = y_{32} + \lambda_{32} + I\xi \tag{16}$$

$$y_{22} - y_{41} - \lambda_{41} - I\xi = 0 \tag{17}$$

$$y_{42} - y_{21} - \lambda_{21} - I\xi = 0 \tag{18}$$

$$y_{22} + \lambda_{22} + I\xi = y_{42} + \lambda_{42} + I\xi = 1 \tag{19}$$

(3) For each movement, the start of the green should be within a fraction between 0 and 1 of the cycle length.

$$1 \geqslant y_{iw}, \quad y^{s}_{iw}, \quad y^{s1}_{iw}, \quad y^{s2}_{iw} \geqslant 0, \qquad \forall i \in \mathcal{L}, \quad w \in \mathcal{T} \tag{20}$$

(4) The green time ratio of a movement should be within a fraction between 0 and 1.

$$1 \geqslant \lambda_{iw} \geqslant 0, \qquad \forall i \in \mathcal{L}, \quad w \in \mathcal{T} \tag{21}$$

(5) The lane signal timings could be defined by the constraints (22), (23). If a lane is shared by more than one movement, these movements must receive identical signal indication to avoid ambiguity. For example, when the approach lane k on leg 1 is not a special lane ($\delta_{11k} = 0$) and the right-turn and through movements are permitted on approach lane k on leg 1, we have $x_{112k} = x_{113k} = 1$; then according to constraint (22), we have $0 \geqslant Y_{1k} - y_{12} \geqslant 0$ and $0 \geqslant Y_{1k} - y_{13} \geqslant 0$; therefore, $g_{12} = g_{13}$. It indicates that the start of green for right-turn and the through movement on leg 1 should be equal. Similarly, the green time ratio for right-turn and the through movement on leg 1 at the main intersection should be the same according to constraint (23).

$$M(1 - x_{i1wk}) \geqslant Y_{ik} - (1 - \delta_{i1k}) y_{iw} - \delta_{i1k} y^{s}_{iw} \geqslant -M(1 - x_{i1wk}), \qquad \forall i \in \mathcal{L}, \quad w \in \mathcal{T}, \quad k \in \{1, \ldots, n_{i1}\} \tag{22}$$

$$M(1 - x_{i1wk}) \geqslant \Lambda_{ik} - (1 - \delta_{i1k}) \lambda_{iw} - \delta_{i1k} \lambda_{iw} \geqslant -M(1 - x_{i1wk}), \qquad \forall i \in \mathcal{L}, \quad w \in \mathcal{T}, \quad k \in \{1, \ldots, n_{i1}\} \tag{23}$$

3.3.3. Capacity adjustment constraints

As illustrated in Fig. 7, the upstream freeway off-ramp may cause negative effect on the downstream intersection approach saturation flow rate due to blockage and weaving. For example, queue at the downstream intersection during the red phase may easily prevent the off-ramp exiting traffic from merging into their target approach lanes, causing waste of capacity of those approach lanes during green time (see Fig. 7b and c). Therefore the saturation flow rate should be adjusted to the weaving flow during this portion of the green.

According to Fig. 7, the capacity of an approach lane k can be estimated with:

$$c_{ik} = s^{o}_{ik} T^{o}_{ik} + s^{u}_{ik} T^{u}_{ik}, \qquad \forall i \in \mathcal{L}, \quad k \in \{1, \ldots, n_{i1}\} \tag{24}$$

where s^{o}_{ik} is the normal saturation flow rate for approach lane k, which is an exogenous input or can be measured in field; s^{u}_{ik} is the weaving segment saturation flow rate for lane k, which can be calculated with methods in HCM2010 (TRB, 2010), given by:

$$s^{u}_{ik} = c_f - 438.2(1 + V_{iR})^{1.6} + 0.251 l_{iw} + 119.8 n_{il}, \qquad \forall i \in \mathcal{L}, \quad k \in \{1, \ldots, n_{i1}\} \tag{25}$$

T^{o}_{ik}, the portion of the green time during which traffic flow discharges with saturation flow rate can be determined with:

$$T^{o}_{ik} = T^{q}_{ik} - Y_{ik}, \qquad \forall i \in \mathcal{L}, \quad k \in \{1, \ldots, n_{i1}\} \tag{26}$$

$$Y_{ik} + \frac{3600 l_i}{h_q s^{o}_{ik}} \xi \geqslant T^{q}_{ik}, \qquad \forall i \in \mathcal{L}, \quad k \in \{1, \ldots, n_{i1}\} \tag{27}$$

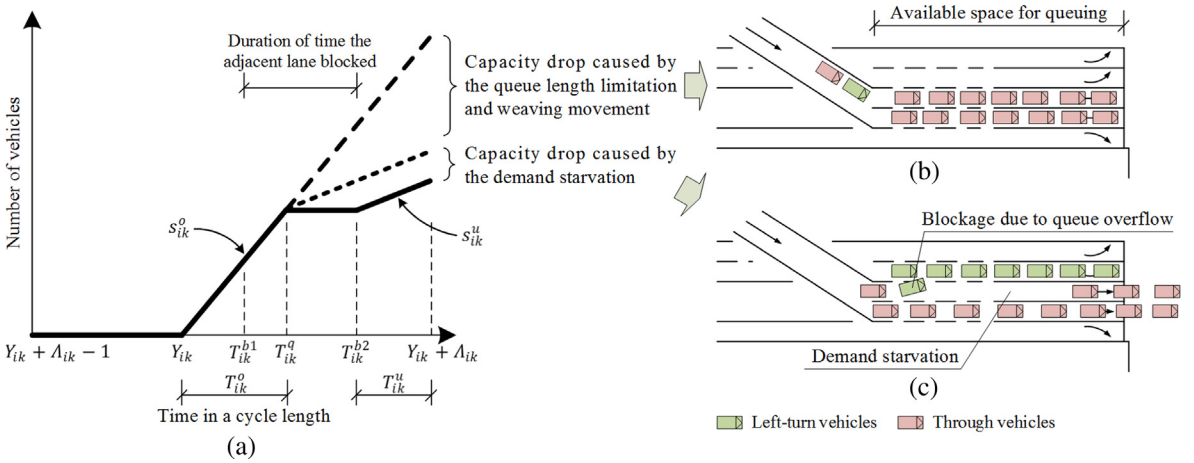

Fig. 7. Impact of upstream off-ramp on downstream intersection approach saturation flow rate.

$$Y_{ik} + \Lambda_{ik} \geqslant T^q_{ik} \geqslant Y_{ik}, \qquad \forall i \in \mathcal{L}, \quad k \in \{1, \ldots, n_{i1}\} \tag{28}$$

and, T^u_{ik}, the portion of the green time during which traffic flow discharges as weaving flow can be determined with:

$$Y_{ik} + \Lambda_{ik} - T^{b2}_{ik} \geqslant T^u_{ik}, \qquad \forall i \in \mathcal{L}, \quad k \in \{1, \ldots, n_{i1}\} \tag{29}$$

$$Y_{ik} + \Lambda_{ik} - T^q_{ik} \geqslant T^u_{ik}, \qquad \forall i \in \mathcal{L}, \quad k \in \{1, \ldots, n_{i1}\} \tag{30}$$

$$\lceil T^{b2}_{ik} - T^{b1}_{ik} \rceil \geqslant T^u_{ik}, \qquad \forall i \in \mathcal{L}, \quad k \in \{1, \ldots, n_{i1}\} \tag{31}$$

$$T^{b1}_{ik} \geqslant Y_{i(k+1)} + \Lambda_{i(k+1)} + \frac{3600 l_i}{h_q \sum_{w \in \mathcal{T}} q_{i1(k+1)w}} \xi + \alpha^{b1}_{ik1}, \qquad \forall i \in \mathcal{L}, \quad k \in \{1, \ldots, n_{i1} - 1\} \tag{32}$$

$$T^{b1}_{ik} \geqslant Y_{i(k-1)} + \Lambda_{i(k-1)} + \frac{3600 l_i}{h_q \sum_{w \in \mathcal{T}} q_{i1(k-1)w}} \xi + \alpha^{b1}_{ik2}, \qquad \forall i \in \mathcal{L}, \quad k \in \{2, \ldots, n_{i1}\} \tag{33}$$

$$T^{b2}_{ik} \geqslant Y_{i(k+1)} + \frac{3600 l_i}{h_q s^o_{i(k+1)}} \xi + \alpha^{b2}_{ik1}, \qquad \forall i \in \mathcal{L}, \quad k \in \{1, \ldots, n_{i1} - 1\} \tag{34}$$

$$T^{b2}_{ik} \geqslant Y_{i(k-1)} + \frac{3600 l_i}{h_q s^o_{i(k-1)}} \xi + \alpha^{b2}_{ik2}, \qquad \forall i \in \mathcal{L}, \quad k \in \{2, \ldots, n_{i1}\} \tag{35}$$

$$Y_{ik} + \Lambda_{ik} \geqslant T^{b1}_{ik}, \quad T^{b2}_{ik} \geqslant Y_{ik} + \Lambda_{ik} - 1, \qquad \forall i \in \mathcal{L}, \quad k \in \{1, \ldots, n_{i1}\} \tag{36}$$

3.3.4. Other operational constraints

It is assumed that traffic demand from the surface street and freeway off-ramp are exogenous input. Then, the total traffic demand is equal to the sum of them, given by:

$$Q^l_{iw} = Q^s_{iw} + Q^f_{iw}, \qquad \forall i \in \mathcal{L}, \quad w \in \mathcal{T} \tag{37}$$

The sum of sub-flows of a movement on different lanes should be equal to the scaled total flow of that movement by the common flow multiplier, given by:

$$Q^l_{iw} = \mu \sum_{k=1}^{n_{i1}} q_{i1kw}, \qquad \forall i \in \mathcal{L}, \quad w \in \mathcal{T} \tag{38}$$

$$Q^s_{iw} = \mu \sum_{k=1}^{n_{i2}} (q_{i2kw} p^s_{i2k}), \qquad \forall i \in \mathcal{L}, \quad w \in \mathcal{T} \tag{39}$$

$$Q^f_{iw} = \mu \sum_{k=1}^{n_{i2}} (q_{i2kw} p^f_{i2k}), \qquad \forall i \in \mathcal{L}, \quad w \in \mathcal{T} \tag{40}$$

When the movement w on lane k is not permitted (i.e., $x_{irwk} = 0$), the assigned lane flow should be equal to 0, given by:

$$M x_{irkw} \geqslant q_{irkw}, \qquad \forall i \in \mathcal{L}, \quad r \in \mathcal{S}, \quad k \in \{1, \ldots, n_{ir}\}, \quad w \in \mathcal{T} \tag{41}$$

The volume of the movement w from lane k at the off-ramp ground point to lane k' at the intersection ($q_{iw(2k,1k')}$) could be determined with:

$$q_{i2kw} \geqslant q_{iw(2k,1k')}, \qquad \forall i \in \mathcal{L}, \quad w \in \mathcal{T}, \quad k \in \{1, \ldots, n_{i2}\}, \quad k' \in \{1, \ldots, n_{i1}\} \tag{42}$$

$$q_{i1k'w} \geqslant q_{iw(2k,1k')}, \qquad \forall i \in \mathcal{L}, \quad w \in \mathcal{T}, \quad k \in \{1, \ldots, n_{i2}\}, \quad k' \in \{1, \ldots, n_{i1}\} \tag{43}$$

$$q_{i2kw} = \sum_{k'=1}^{n_{i1}} q_{iw(2k,1k')}, \qquad \forall i \in \mathcal{L}, \quad w \in \mathcal{T}, \quad k \in \{1, \ldots, n_{i2}\} \tag{44}$$

$$q_{i1k'w} = \sum_{k=1}^{n_{i2}} q_{iw(2k,1k')}, \qquad \forall i \in \mathcal{L}, \quad w \in \mathcal{T}, \quad k' \in \{1, \ldots, n_{i1}\} \tag{45}$$

The weaving volume ratio, which is a key parameter in calculating the weaving segment saturation flow rate as shown in constraint (46), can be determined with:

$$V_{iR} = \frac{\sum_{w\in\mathcal{T}}\sum_{k=1}^{n_{i2}}\sum_{k'=1}^{n_{i1}} q^u_{iw(2k,1k')}}{\sum_{w\in\mathcal{T}} Q^I_{iw}}, \qquad \forall i \in \mathcal{L} \tag{46}$$

The weaving flow of the movement w from lane k at the off-ramp ground point to lane k' at the intersection ($q^u_{iw(2k,1k')}$) could be determined with:

$$q^u_{iw(2k,1k')} \geqslant q_{iw(2k,1k')} + M(\eta_{iw(2k,1k')} - 1), \qquad \forall i \in \mathcal{L}, \quad w \in \mathcal{T}, \quad k \in \{1,\ldots,n_{i2}\}, \quad k' \in \{1,\ldots,n_{i1}\} \tag{47}$$

$$q_{iw(2k,1k')} \geqslant q^u_{iw(2k,1k')} \geqslant 0, \qquad \forall i \in \mathcal{L}, \quad w \in \mathcal{T}, \quad k \in \{1,\ldots,n_{i2}\}, \quad k' \in \{1,\ldots,n_{i1}\} \tag{48}$$

Additionally, constraint (49) indicates whether the movement w from lane k at the off-ramp ground point to lane k' at the intersection is a potential weaving movement, given by:

$$M\left(\sum_{j'=k+1}^{n_{i1}}\sum_{j=1}^{k-1} q_{iw(2j,1j')} + \sum_{j'=1}^{k-1}\sum_{j=k+1}^{k=n_{i2}} q_{iw(2j,1j')}\right) \geqslant \eta_{iw(2k,1k')} \geqslant \frac{1}{M}\left(\sum_{j'=k+1}^{n_{i1}}\sum_{j=1}^{k-1} q_{iw(2j,1j')} + \sum_{j'=1}^{k-1}\sum_{j=k+1}^{k=n_{i2}} q_{iw(2j,1j')}\right),$$
$$\forall i \in \mathcal{L}, \quad w \in \mathcal{T}, \quad k \in \{1,\ldots,n_{i2}\}, \quad k' \in \{1,\ldots,n_{i1}\} \tag{49}$$

Last but not least, to ensure that the intersection and the upstream off-ramp area operate reasonably well, the degree of saturation of every traffic lane should be limited by a maximum acceptable value.

$$d_{\max} c_{ik} \geqslant \sum_{w\in\mathcal{T}} q_{i1kw}, \qquad \forall r \in N, \quad i \in A, \quad k \in \{1,\ldots,n_{if}+n_{ir}\} \tag{50}$$

3.4. Solution

The optimization model presented above is a mixed-integer non-linear program with the objective function of Eq. (1) and constraints (1)–(50). In solving the program, the following three problems should be addressed. Then, the model could be transformed into a mix-integer linear program which can be solved by the standard branch-and-bound technique. The number of decision variables is related to the number of lanes on each leg and can be estimated with $2\sum_{i\in\mathcal{L}} n_{i1}n_{i2} + 4\sum_{i\in\mathcal{L}}\sum_{r\in\mathcal{S}} n_{ir} + 58$. For a four-leg intersection with five lanes on each leg and an off-ramp on one leg, the total number of decision variables is 208, which can be readily handled by any commercial MILP solver (e.g. Lingo).

3.4.1. Linearization of the products of binary variables in constraints (2)–(7)

The products of binary variables, $\delta_{iww'}$, are involved in constraints (2)–(7). This type of problem can be transformed into a mix-integer linear equation by adding two more constraints (Abraham et al., 2009; Fu, 2007).

Constraint (2) could be rewritten as:

$$\delta_{i12} + (1-\delta_{i13}) + (1-\delta_{i23}) - \beta_{i1} \leqslant 2, \qquad \forall i \in \mathcal{L} \tag{51}$$

$$-\delta_{i12} - (1-\delta_{i13}) - (1-\delta_{i23}) + 3\beta_{i1} \leqslant 0, \qquad \forall i \in \mathcal{L} \tag{52}$$

Constraint (3) could be rewritten as:

$$(1-\delta_{i12}) + (1-\delta_{i13}) + \delta_{i23} - \beta_{i2} \leqslant 2, \qquad \forall i \in \mathcal{L} \tag{53}$$

$$-(1-\delta_{i12}) - (1-\delta_{i13}) - \delta_{i23} + 3\beta_{i2} \leqslant 0, \qquad \forall i \in \mathcal{L} \tag{54}$$

Constraint (4) could be rewritten as:

$$\delta_{i12} + \delta_{i13} + (1-\delta_{i23}) - \beta_{i3} \leqslant 2, \qquad \forall i \in \mathcal{L} \tag{55}$$

$$-\delta_{i12} - \delta_{i13} - (1-\delta_{i23}) + 3\beta_{i3} \leqslant 0, \qquad \forall i \in \mathcal{L} \tag{56}$$

Constraint (5) could be rewritten as:

$$\delta_{i12} + (1-\delta_{i13}) + \delta_{i23} - \beta_{i4} \leqslant 2, \qquad \forall i \in \mathcal{L} \tag{57}$$

$$-\delta_{i12} - (1-\delta_{i13}) - \delta_{i23} + 3\beta_{i4} \leqslant 0, \qquad \forall i \in \mathcal{L} \tag{58}$$

Constraint (6) could be rewritten as:

$$(1-\delta_{i12}) + \delta_{i13} + \delta_{i23} - \beta_{i5} \leqslant 2, \qquad \forall i \in \mathcal{L} \tag{59}$$

$$-(1-\delta_{i12})-\delta_{i13}-\delta_{i23}+3\beta_{i5}\leqslant 0,\qquad \forall i\in\mathcal{L} \tag{60}$$

Constraint (7) could be rewritten as:

$$\delta_{i12}+\delta_{i13}+\delta_{i23}-\beta_{i6}\leqslant 2,\qquad \forall i\in\mathcal{L} \tag{61}$$

$$-\delta_{i12}-\delta_{i13}-\delta_{i23}+3\beta_{i6}\leqslant 0,\qquad \forall i\in\mathcal{L} \tag{62}$$

3.4.2. Linearization of the lane signal timings constraints

The products of two decision variables, $\delta_{i1k}y_{iw}$ and $\delta_{i1k}y^s_{iw}$, are involved in the lane signal timings constraints (22) and (23) because we should differentiate the normal movements and conflicting movements. This type of problem can be transformed into a mix-integer linear equation by expanding constraints (22) and (23) to the following ten constraints. Constraints (63) and (64) will be active only when the approach lane is not a special lane ($\delta_{i1k}=0$). For example, when the movement w is permitted on the approach lane k on leg i ($x_{i1wk}=1$) and the approach lane is not a special lane ($\delta_{i1k}=0$), we have $(1-x_{i1wk}+\delta_{i1k})=0$. According to constraint (63), we have $0\geqslant Y_{ik}-y_{iw}\geqslant 0$; so $Y_{ik}=y_{iw}$. Otherwise, if the approach lane is a special lane ($\delta_{i1k}=1$), we have $(1-x_{i1wk}+\delta_{i1k})=1$. According to constraint (63), we have $M\geqslant Y_{ik}-y_{iw}\geqslant -M$; it will always be satisfied. Constraints (65)–(72) will be active only when the approach lane is a special lane ($\delta_{i1k}=1$). For left-turn and right-turn special lane, constraints (65) and (69) will be used. For through special lane, constraints (66)–(68) and (70)–(72) will be used.

For normal movements:

$$M(1-x_{i1wk}+\delta_{i1k})\geqslant Y_{ik}-y_{iw}\geqslant -M(1-x_{i1wk}+\delta_{i1k}),\qquad \forall i\in\mathcal{L},\quad w\in\mathcal{T},\quad k\in\{1,\ldots,n_{i1}\} \tag{63}$$

$$M(1-x_{i1wk}+\delta_{i1k})\geqslant \Lambda_{ik}-\lambda_{iw}\geqslant -M(1-x_{i1wk}+\delta_{i1k}),\qquad \forall i\in\mathcal{L},\quad w\in\mathcal{T},\quad k\in\{1,\ldots,n_{i1}\} \tag{64}$$

For conflicting movements:

$$M(2-x_{i1wk}-\delta_{i1k})\geqslant Y_{ik}-y^s_{iw}\geqslant -M(2-x_{i1wk}-\delta_{i1k}),\qquad \forall i\in\{3\},\quad w\in\{1,3\},\quad k\in\{1,\ldots,n_{i1}\} \tag{65}$$

$$M(2-x_{i1wk}-\delta_{i1k}+\beta_{i4}+\beta_{i6})\geqslant Y_{ik}-y^s_{iw}\geqslant -M(2-x_{i1wk}-\delta_{i1k}+\beta_{i4}+\beta_{i6}),\qquad \forall i\in\{3\},\quad w\in\{2\},\quad k\in\{1,\ldots,n_{i1}\} \tag{66}$$

$$M(3-x_{i1wk}-\beta_{i4}-\beta_{i6}-\sum_{k'=k+1}^{n_{i1}}x_{i11k'})\geqslant Y_{ik}-y^{s1}_{iw}\geqslant -M(3-x_{i1wk}-\beta_{i4}-\beta_{i6}-\sum_{k'=k+1}^{n_{i1}}x_{i11k'}),$$
$$\forall i\in\{3\},\quad w\in\{2\},\quad k\in\{1,\ldots,n_{i1}-1\} \tag{67}$$

$$M(3-x_{i1wk}-\beta_{i4}-\beta_{i6}-\sum_{k'=1}^{k-1}x_{i13k'})\geqslant Y_{ik}-y^{s2}_{iw}\geqslant -M(3-x_{i1wk}-\beta_{i4}-\beta_{i6}-\sum_{k'=1}^{k-1}x_{i13k'}),$$
$$\forall i\in\{3\},\quad w\in\{2\},\quad k\in\{2,\ldots,n_{i1}\} \tag{68}$$

$$M(2-x_{i1wk}-\delta_{i1k})\geqslant \Lambda_{ik}-\lambda^s_{iw}\geqslant -M(2-x_{i1wk}-\delta_{i1k}),\qquad \forall i\in\{3\},\quad w\in\{1,3\},\quad k\in\{1,\ldots,n_{i1}\} \tag{69}$$

$$M(2-x_{i1wk}-\delta_{i1k}+\beta_{i4}+\beta_{i6})\geqslant \Lambda_{ik}-\lambda^s_{iw}\geqslant -M(2-x_{i1wk}-\delta_{i1k}+\beta_{i4}+\beta_{i6}),\qquad \forall i\in\{3\},\quad w\in\{2\},\quad k\in\{1,\ldots,n_{i1}\} \tag{70}$$

$$M(3-x_{i1wk}-\beta_{i4}-\beta_{i6}-\sum_{k'=k+1}^{n_{i1}}x_{i11k'})\geqslant \Lambda_{ik}-\lambda^{s1}_{iw}\geqslant -M(3-x_{i1wk}-\beta_{i4}-\beta_{i6}-\sum_{k'=k+1}^{n_{i1}}x_{i11k'}),$$
$$\forall i\in\{3\},\quad w\in\{2\},\quad k\in\{1,\ldots,n_{i1}-1\} \tag{71}$$

$$M(3-x_{i1wk}-\beta_{i4}-\beta_{i6}-\sum_{k'=1}^{k-1}x_{i13k'})\geqslant \Lambda_{ik}-\lambda^{s2}_{iw}\geqslant -M(3-x_{i1wk}-\beta_{i4}-\beta_{i6}-\sum_{k'=1}^{k-1}x_{i13k'}),$$
$$\forall i\in\{3\},\quad w\in\{2\},\quad k\in\{2,\ldots,n_{i1}\} \tag{72}$$

3.4.3. Explicit expression of phase plan for conflicting movements

For conflicting movements, the start of green and green time ratio should be adjusted according to Fig. 4.

$$M(1-\beta_{31}-\beta_{33}-\beta_{34}-\beta_{35}-\beta_{36})\geqslant y^s_{31}-y_{31}\geqslant M(\beta_{31}+\beta_{33}+\beta_{34}+\beta_{35}+\beta_{36}-1) \tag{73}$$

$$y_{12} - y_{31}^s - \lambda_{31}^s - I\xi \geqslant M(\beta_{31} + \beta_{33} + \beta_{34} + \beta_{35} + \beta_{36} - 1) \tag{74}$$

$$y_{32}^s - y_{11} - \lambda_{11} - I\xi \geqslant M(\beta_{31} + \beta_{32} + \beta_{33} + \beta_{34} + \beta_{36} - 1) \tag{75}$$

$$y_{32}^s - y_{31}^s - \lambda_{31}^s - I\xi \geqslant M(\beta_{31} + \beta_{32} + \beta_{33} + \beta_{34} + \beta_{36} - 1) \tag{76}$$

$$M(1 - \beta_{31} - \beta_{32} - \beta_{33} - \beta_{34} - \beta_{36}) \geqslant y_{32}^s + \lambda_{32}^s - y_{32} - \lambda_{32} \geqslant M(\beta_{31} + \beta_{32} + \beta_{33} + \beta_{34} + \beta_{36} - 1) \tag{77}$$

$$M(1 - \beta_{35}) \geqslant y_{32}^s - y_{32} \geqslant M(\beta_{35} - 1) \tag{78}$$

$$y_{32} + \lambda_{32} - y_{32}^s - \lambda_{32}^s \geqslant M(\beta_{35} + \beta_{36} - 1) \tag{79}$$

$$y_{33}^s - y_{31}^s - \lambda_{31}^s - I\xi \geqslant M(\beta_{33} + \beta_{35} + \beta_{36} - 1) \tag{80}$$

$$y_{33}^s - y_{32}^s - \lambda_{32}^s - I\xi \geqslant M(\beta_{35} + \beta_{36} - 1) \tag{81}$$

4. Case study

In this section, we evaluate the performance of the proposed model through a case study and extensive numerical tests. The optimization results obtained from the proposed integrated design model will be compared with conventional plans (obtained by proposed model without the consideration of non-traditional lane assignment). Sensitivity analysis will also be conducted to identify the conditions for best application of the proposed model.

4.1. The study site

The No. 18 off-ramp (the Guoding Rd. exit) of the Middle ring expressway in Shanghai, China, its downstream intersection (Handan Rd. - Guoding Rd. intersection), and their connecting segment are used to validate and evaluate the effectiveness of the proposed integrated model. The original layout of the study site is illustrated in Fig. 8. The off-ramp connects to Handan Rd. at 60 m upstream of the EB stop line. Aggregated traffic demand at the test site during peak hours is summarized in Table 3. Other parameters used in the case study are summarized in Table 4.

Currently, since the weaving section between the stop line and off-ramp ground point is only 60 m, there is very limited space for traffic weaving between off-ramp and the surface street, resulting in severe blockage and spillover problems.

4.2. Results and discussions

The proposed model is implemented at the study site to design lane markings and signal timings. The optimized lane markings are illustrated in Fig. 9. Signal timings in both morning and evening peak hours under the conventional design and the proposed model are summarized and compared in Table 5. The microscopic simulation package VISSIM 5.40 is used and calibrated as the unbiased evaluator to evaluate the performance of the proposed model in comparison with the

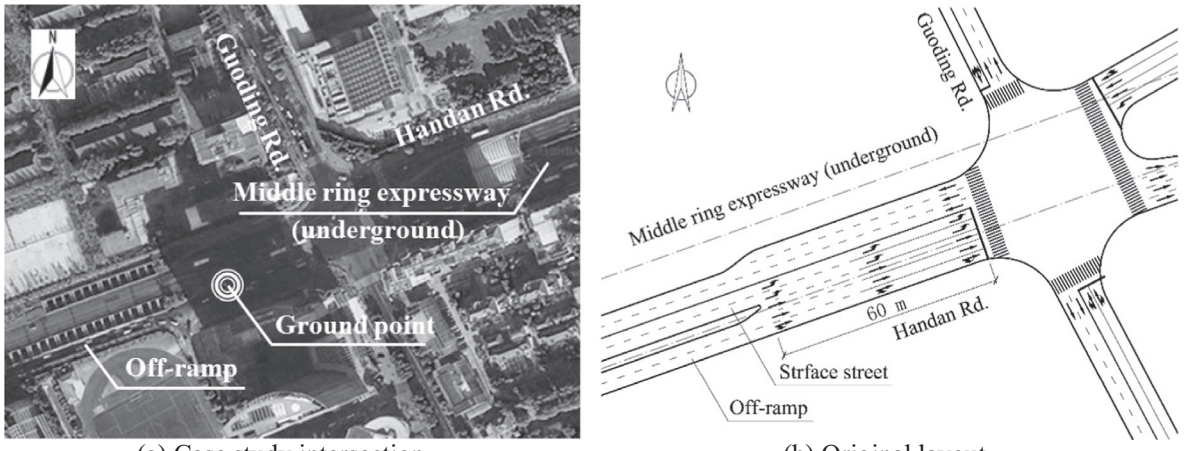

(a) Case study intersection (b) Original layout

Fig. 8. The study site and its original geometric layout.

Table 3
Aggregated traffic demand at the study site (veh/h).

Time-of-day	WB			EB						NB			SB			Freeway mainline
	L	T	R	L-S	T-S	R-S	L-R	T-R	R-R	L	T	R	L	T	R	
Morning peak hours	188	445	154	213	505	74	233	575	102	55	352	49	43	410	111	3016
Evening peak hours	197	604	156	244	624	111	275	710	129	62	366	61	54	307	63	3137

Note: The abbreviations EB, WB, NB, and SB refer to eastbound, westbound, northbound, and southbound, respectively. Abbreviations L, T, and R indicate the left-turn, through movement, and right-turn, respectively. Abbreviations -S and -R indicate the movement from surface streets and from off-ramp.

Table 4
Parameters used in the case study.

Input parameters	Value	Input parameters	Value
Maximum cycle length, C_{max}	120 s	Minimum cycle length, C_{min}	60 s
Clearance time for a pair of conflicting traffic movements, I	4 s	Average space headway for queuing vehicles, h_q	7 m
Saturation flow rate on lane k on leg i, s_{ik}^{o}	1800 veh/h/ln	Capacity of a basic segment under ideal conditions per lane, c_f	1800 veh/h/ln
Maximum acceptable degree of the saturation, d_{max}	0.9		

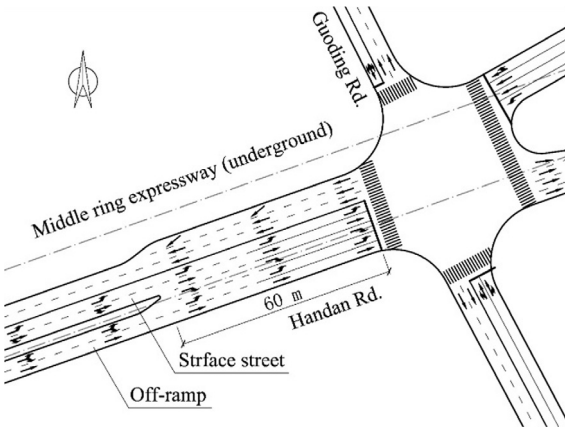

Fig. 9. Lane assignment of the study site.

conventional design. According to the saturation flow rate obtained from field survey (1800 veh/h/ln), the inputs and settings of running the traffic simulation are: the average standstill distance is set to 2.3 m; additive part of safety distance is set to 2.3 m; multiplicative part of safety distance is set to 3.3 m; the desired speed is set to 40 km/h. Results averaged from 20 simulation runs are used for evaluation to overcome the randomness. Two performance indicators, the total throughput and the average vehicular delay, are used for comparison (see Table 6 for results).

It can be observed from Table 6 that the total throughputs of the intersection under the conventional design and Synchro design are less than the total intersection demand during both morning and evening peak hours (morning: 3340 vehs and 3290 vehs < 3509 vehs, evening: 3487 vehs and 3407 vehs < 3963 vehs), indicating the oversaturated traffic condition with the conventional design. This is also validated by the average vehicular delay under the conventional design (61.7 s and 111.6 s for morning and evening peak hours, respectively). Comparison results show that the proposed model can significantly improve the traffic operational performance at the study site (17.32% and 52.35% reduction in average delay during morning and evening peak hours) and maintain its under-saturated condition without the need of lane addition and intersection expansion, which demonstrates the cost-effectiveness of the proposed model. Furthermore, as the result of the performance improvement of the intersection, the off-ramp queue spillover problem was mitigated. The travel delay along the freeway mainline was significantly reduced accordingly (93.27% and 95.76% reduction in average delay during morning and evening peak hours).

4.3. Sensitivity analyses

To further investigate the performance of the proposed model under various geometric configurations and demand levels, extensive sensitivity analyses are performed. A total of 18 experimental scenarios are designed (summarized in Table 7) with

Table 5
Signal timing plans.

Time-of-day	Plan	Signal timing	WB			EB						NB			SB		
			L	T	R	L-S	T-S	R-S	L-R	T-R	R-R	L	T	R	L	T	R
Morning peak hours	Conventional	Cycle length (s)	120														
		Start of green (s)	0	28	28	0	18	18	–	–	–	53	53	53	74	74	74
		Duration of green (s)	14	21	21	24	31	31	–	–	–	17	17	17	42	42	42
		End of green (s)	14	49	49	24	49	49	–	–	–	70	70	70	116	116	116
	Synchro	Cycle length (s)	90														
		Start of green (s)	0	19	19	0	14	14	–	–	–	70	70	70	39	39	39
		Duration of green (s)	10	16	16	15	21	21	–	–	–	16	16	16	27	27	27
		End of green (s)	10	35	35	15	35	35	–	–	–	86	86	86	66	66	66
	Optimal design	Cycle length (s)	120														
		Start of green (s)	0	30	30	0	20	59	0	16	59	59	59	59	78	78	78
		Duration of green (s)	12	25	25	26	35	15	16	39	15	15	15	15	38	38	38
		End of green (s)	12	55	55	26	55	74	16	55	74	74	74	74	116	116	116
Evening peak hours	Conventional	Cycle length (s)	120														
		Start of green (s)	0	31	31	0	19	19	–	–	–	62	62	62	84	84	84
		Duration of green (s)	15	27	27	27	39	39	–	–	–	18	18	18	32	32	32
		End of green (s)	15	58	58	27	58	58	–	–	–	80	80	80	116	116	116
	Synchro	Cycle length (s)	90														
		Start of green (s)	0	23	23	0	15	15	–	–	–	70	70	70	46	46	46
		Duration of green (s)	11	19	19	19	27	27	–	–	–	16	16	16	20	20	20
		End of green (s)	11	42	42	19	42	42	–	–	–	86	86	86	66	66	66
	Optimal design	Cycle length (s)	120														
		Start of green (s)	0	33	33	0	22	68	0	17	68	68	68	68	88	88	88
		Duration of green (s)	13	31	31	29	42	16	18	47	16	16	16	16	28	28	28
		End of green (s)	13	64	64	29	64	84	18	64	84	84	84	84	116	116	116

variation of the number of lanes on major streets, the distances between the stop line and the off-ramp, and the locations of the off-ramp. Traffic demand varies in proportional to the number of lanes. The turning proportions of the left-turn and through movements are set to vary from 20% to 60%. All other model parameters are kept the same as in Section 4.1.

Fig. 10 summarizes the evaluation results for all experimental scenarios. For each picture, the horizontal and vertical axes represent the proportion of the left-turn and through movements, respectively; and the contour lines illustrate the percentage of capacity improvement of the proposed model over the conventional design. Fig. 11 summarizes the variation of capacity improvement with affecting factors. The following findings can be reached:

(1) Overall, the proposed model outperforms the conventional design in terms of capacity under all tested scenarios (up to 30% capacity improvement than the conventional design).
(2) Capacity improvement with off-ramp located at the middle of the road cross section is always slightly higher than that with off-ramp located the left most road cross section under all numerical cases discussed in the paper. Paired *t*-test results (see Table 8a) show the significant difference between the capacity improvement when off-ramp located at the left most of the road cross section and the capacity improvement when off-ramp located at the middle of the road cross section ($t = -5.350$, p-value = 0.000 < 0.05), indicating that the off-ramp connected to the surface street at the middle of the road cross section has a better performance. Table 8b further investigates the capacity improvement under different locations of off-ramps combined with multiple affecting factors. The difference is more pronounced when the distances between the stop line and off-ramp is short (50 m), the number of lanes is few, and the turning proportions is medium (0.3–0.45).
(3) From row sub-figures, one can observe that the capacity improvement decreases with the increase of the distances between the stop line and the off-ramp. Longer distance between the stop line and the off-ramp leads to more space to hold the queue and flexibility for traffic weaving. It is also noticeable that there is no significant advantage using the proposed design when the distance between the stop line and off-ramp is longer than 150 m.
(4) From the column sub-figures, it can be found that the capacity improvement over the conventional design increases with the number of lanes on the surface street (capacity increases 3.24%, 5.38%, and 6.04% when the number of lanes on surface streets increases from two to four, respectively). This is due to the fact that more lanes may increase the complexity of weaving between freeway and surface street traffic under the conventional design, causing more traffic congestion and worse utilization of the intersection capacity; however non-traditional lane assignment strategy can retain the higher capacity offered by the increasing number of lanes while effectively mitigate or prevent traffic weaving complexities.
(5) From each sub-figure, more significant improvement in capacity could be obtained when the right-turn proportion is low (i.e. left-turn proportion plus through movement proportion is high). It is due to the fact that the right-turn-on-red (RTOR) is used, which reduces the impact of the weaving and queue overflow problem caused by the right-turn traffic.

Table 6
Comparison of operational performance.

Time-of-day	Leg	Movement	Throughput (veh)				Delay (s)			
			C_d	Sy	P_m	Im (%)	C_d	Sy	P_m	I (%)
Morning peak hours	WB	L	186	178	188	1.08	54.5	54.8	66.5	22.02
		T	444	450	449	1.13	46.7	34.3	40.8	−12.63
		R	157	160	158	0.64	42.9	34.4	37.1	−13.52
	EB	L-S	203	208	217	6.90	49.7	45.8	41.6	−16.30
		T-S	451	437	508	12.64	83.1	90.5	58	−30.20
		R-S	65	60	72	10.77	87	92.9	59.4	−31.72
		L-R	207	192	232	12.08	87.6	92.7	61.7	−29.57
		T-R	524	503	580	10.69	81	88.3	45.9	−43.33
		R-R	88	93	95	7.95	56.3	60.7	49.1	−12.79
	NB	L	53	54	53	0.00	53.9	51.4	56.6	5.01
		T	352	354	354	0.57	51.1	46.2	55.7	9.00
		R	46	43	45	−2.17	53.9	49.7	57.7	7.05
	SB	L	48	47	47	−2.08	42.8	34.9	46.8	9.35
		T	403	397	399	−0.99	48.1	42.8	53.1	10.40
		R	113	114	113	0.00	43.5	45.2	46.6	7.13
	Overall intersection		3340	3290	3510	5.09	61.7	60.3	51.0	−17.32
	Freeway mainline		2915	2902	3020	3.60	55.0	58.3	3.7	−93.27
Evening peak hours	WB	L	189	192	190	0.53	55.6	48.7	68.9	23.92
		T	598	610	609	1.84	41.3	31.0	39.4	−4.60
		R	152	153	155	1.97	45.5	34.0	38	−16.48
	EB	L-S	199	204	238	19.60	156.4	143.0	49.7	−68.22
		T-S	492	469	627	27.44	188.1	206.2	62.5	−66.77
		R-S	89	79	118	32.58	179.2	190.9	78.4	−56.25
		L-R	204	176	274	34.31	190.3	233.7	67.1	−64.74
		T-R	549	517	715	30.24	191	210.1	41	−78.53
		R-R	103	104	124	20.39	161.5	162.2	62.9	−61.05
	NB	L	62	63	60	−3.23	50.9	44.8	61.6	21.02
		T	365	362	373	2.19	53.8	41.1	55.8	3.72
		R	55	56	55	0.00	48.1	44.9	55.8	16.01
	SB	L	58	58	57	−1.72	50.6	52.7	55.4	9.49
		T	305	298	308	0.98%	49.8	54.7	57.7	15.86
		R	67	66	66	−1.49	52.2	54.1	57.7	10.54
	Overall intersection		3487	3407	3969	13.82	111.6	112.8	53.2	−52.35
	Freeway mainline		2669	2476	3142	17.72	106.2	169.6	4.5	−95.76

Note: The abbreviations C_d, Sy, P_m, and Im refer to Conventional design, Synchro, Proposed model, and improvement of the proposed model over the conventional design, respectively.

Table 7
Experimental scenarios for sensitivity analysis.

Scenarios	Number of lanes on surface street	Number of lanes on crossing street	Number of lanes of off-ramp	Distance between the stop line and off-ramp (m)	Location of the off-ramp
1	2	2	2	50	Located at the left most of the road cross section
2	2	2	2	100	
3	2	2	2	150	
4	3	2	2	50	
5	3	2	2	100	
6	3	2	2	150	
7	4	2	2	50	
8	4	2	2	100	
9	4	2	2	150	
10	2	2	2	50	Located at the middle of the road cross section
11	2	2	2	100	
12	2	2	2	150	
13	3	2	2	50	
14	3	2	2	100	
15	3	2	2	150	
16	4	2	2	50	
17	4	2	2	100	
18	4	2	2	150	

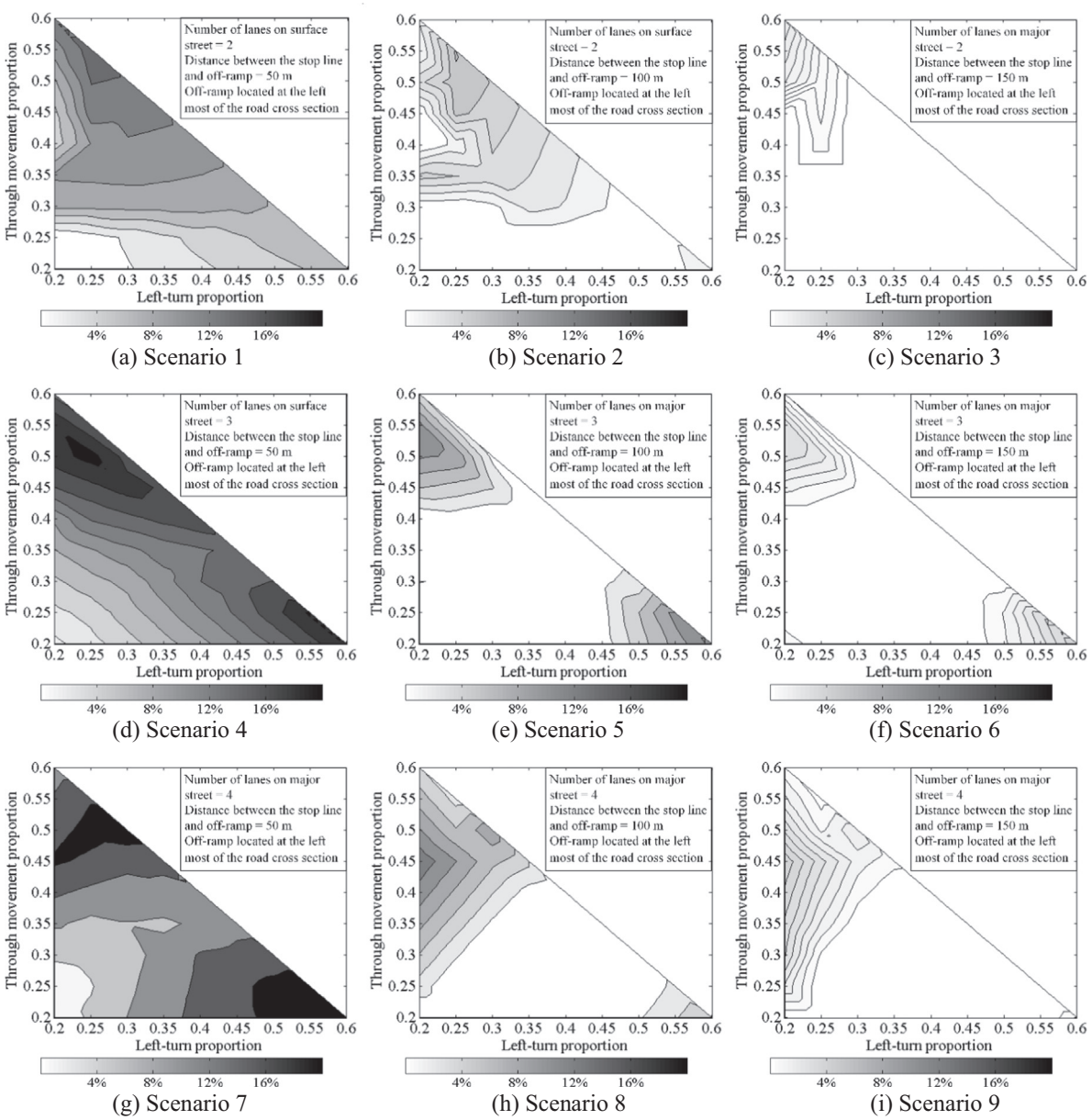

Fig. 10. Percentage of capacity improvement of by the proposed model under various experimental scenarios.

5. Conclusions

An integrated design model for non-traditional lane assignment and signal optimization at the off-ramp, its downstream intersection, and their connecting segment is presented in this paper to mitigate or eliminate traffic weaving and to maximize the section's overall capacity. Traditional channelization restrictions (e.g. left-turn lanes should be located at the left side of the through lanes) are relaxed. A mixed-integer non-linear program model is formulated to capture real-world operational constraints regarding the non-traditional lane assignment, special phasing treatment and signal timing. The mathematical model is linearized and solved by the standard branch-and-bound technique. Extensive numerical analysis and case studies were conducted to evaluate the performance of the proposed model in comparison with conventional design under different geometric and traffic demand pattern scenarios. The following conclusions can be drawn:

(1) The non-traditional lane assignment strategy can significantly improve the traffic operational performance of the off-ramp and downstream intersection integrated section (up to 30% capacity improvement) and mitigate the off-ramp queue spillover problem. The travel delay along the freeway mainline could be significantly reduced accordingly.

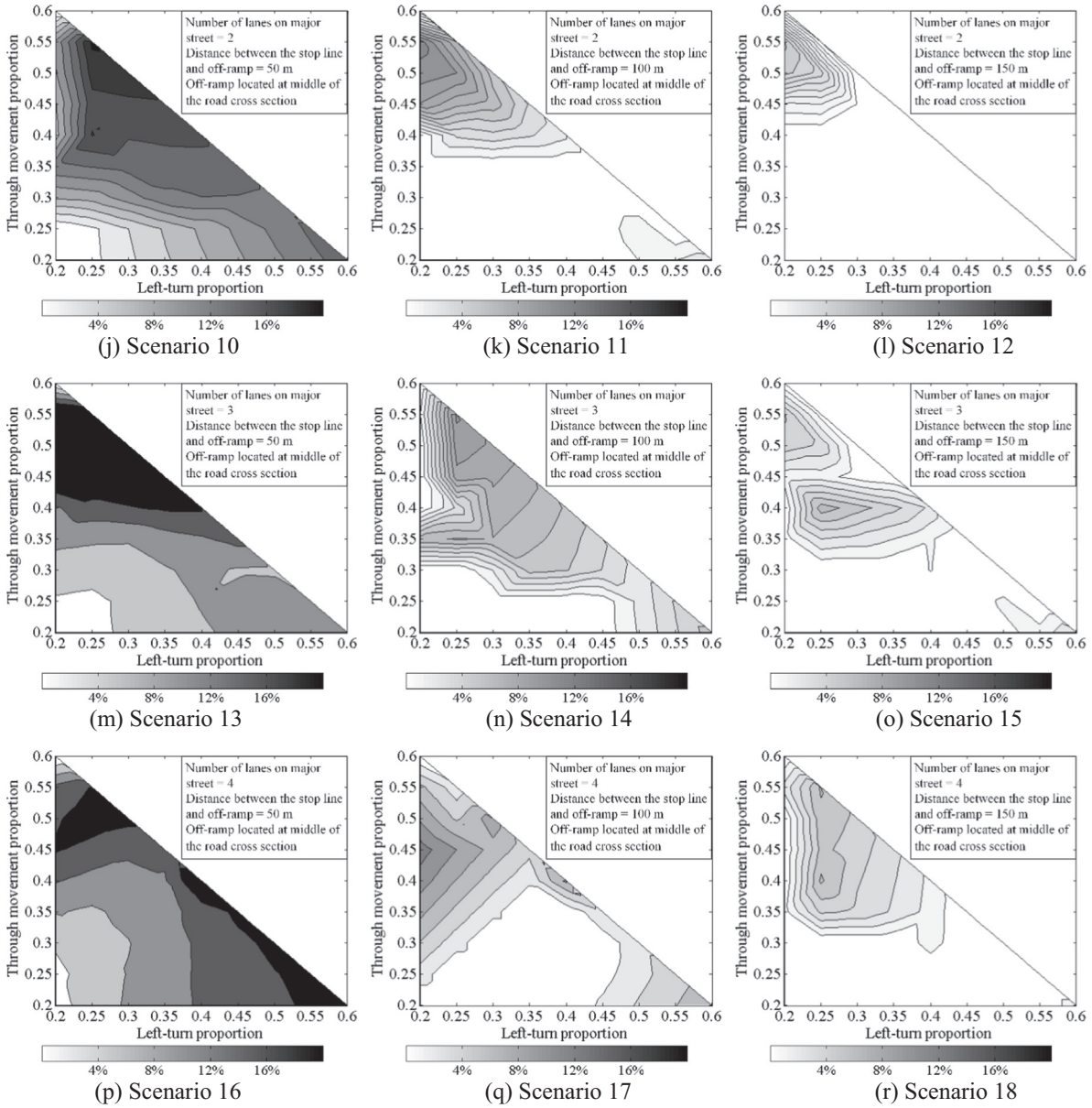

Fig. 10 (*continued*)

(2) The proposed model is applicable when the distance between the stop line and off-ramp is less than 150 m. The capacity improvement from the integrated design model decreases with the increase of the distances between the stop line and the off-ramp and no significant advantage exists when the distance between the stop line and off-ramp is longer than 150 m.

(3) More significant improvement in capacity could be obtained from the integrated design model when the off-ramp is located at the middle of the road cross section (capacity increases 5.78% and 4.89% when the off-ramp is located at the middle of the road cross section and located at the left most road cross section, respectively), more number of lanes is available (capacity increases 3.24%, 5.38%, and 6.04% when the number of lanes on surface streets increases from two to four, respectively) and the right-turn proportion is low (less than 40%).

Note that the advantages of the proposed model depend on the driver's reaction and capacity of short waving sections. These issues themselves are separate research topics and deserve rigorous and extensive research efforts. This study adopted well-established results from previous studies on driver behaviors and weaving capacity. The models and the optimization

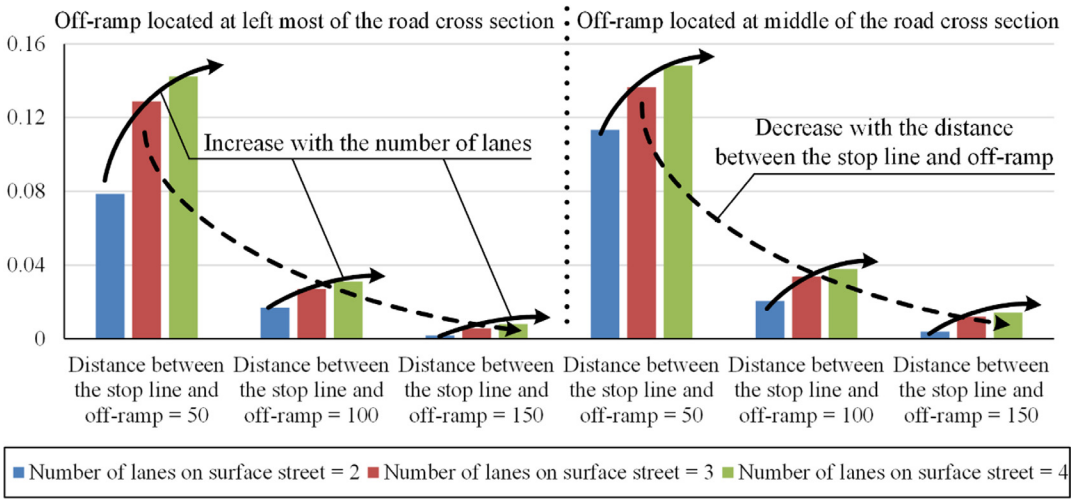

Fig. 11. Capacity improvement with respect to affecting factors.

Table 8
Impact of off-ramp locations on model's performance.

Paired difference											
	Mean	Std. deviation	Std. error mean	95% Confidence interval of the difference		t	df	Sig. (2-tailed)			
				Lower	Upper						
(a)											
Pair: LCS – MCS	−0.00888	0.03339	0.00166	−0.01214	−0.00561	−5.350	404	0.000			
Factors	Distances between the stop line and off-ramp			Number of lanes on major streets			Left-turn proportions			Through movement proportions		
(b)												
Cases	50	100	150	2	3	4	<0.3	0.3–0.45	>0.45	<0.3	0.3–0.45	>50%
LCS	11.7%	2.5%	0.5%	3.2%	5.4%	6.0%	4.9%	4.2%	6.3%	3.8%	5.4%	7.8%
MCS	13.3%	3.1%	1.0%	4.6%	6.1%	6.7%	5.8%	5.5%	6.6%	3.9%	7.5%	8.7%
Increase	1.6%	0.6%	0.5%	1.3%	0.7%	0.7%	0.9%	1.3%	0.3%	0.1%	2.1%	0.9%

Note: The abbreviations LCS and MCS refer to the capacity improvement when off-ramp located at the left most of the road cross section and the capacity improvement when off-ramp located at the middle of the road cross section, respectively.

framework proposed in this study have the flexibility to incorporate new research results/progress. Moreover, careful driving behavior studies and driver education are still needed for its further application, which is the direction of our future study.

Acknowledgements

The research is supported by the National Natural Science Foundation of China under Grant No. 51608324.

References

Abraham, A., Hassanien, A.E., Siarry, P., Engelbrecht, A., 2009. Foundations of Computational Intelligence Volume 3: Global Optimization. Springer, Berlin, Germany.
Cantarella, G.E., Pavone, G., Vitetta, A., 2006. Heuristics for urban road network design: lane layout and signal settings. Eur. J. Oper. Res. 175 (3), 1682–1695.
Cassidy, M.J., Anani, S.B., Haigwood, J.M., 2002. Study of freeway traffic near an off-ramp. Transport. Res. Part A: Pol. Pract. 36 (6), 563–572.
Chen, X., Qi, Y., Li, D., Wang, Y., 2014. Dual right-turn lanes in mitigating weaving conflicts at frontage road intersections in proximity to off-ramps. Transport. Plan. Technol. 37 (3), 307–319.
Cheu, R.L., Jin, X., Ng, K.C., Ng, Y.L., Srinivasan, D., 1998. Calibration of FRESIM for Singapore Expressway using genetic algorithm. J. Transport. Eng.-ASCE 124 (6), 526–535.
Daganzo, C.F., Cassidy, M.J., Bertini, R.L., 1999. Possible explanations of phase transitions in highway traffic. Transport. Res. Part A: Pol. Pract. 33 (5), 365–379.
Daganzo, C.F., Laval, J., Muñoz, J.C., 2002. Ten Strategies for Freeway Congestion Mitigation with Advanced Technologies. University of California, Berkeley, California, USA.
Denney, R.W., Curtis, E., Head, L., 2009. Long green times and cycles at congested traffic signals. Transport. Res. Rec.: J. Transport. Res. Board 2128, 1–10.
Fu, J.L., 2007. Operational Research Methodology and Model. Fudan University Press, Shanghai, China.

Günther, G.E., Coeymans, J.E., Mu09oz, J.C., Herrera, J.C., 2012. Mitigating freeway off-ramp congestion: a surface streets coordinated approach. Transport. Res. Part C: Emerg. Technol. 20 (1), 27–43.
Gallivan, S., Heydecker, B., 1988. Optimising the control performance of traffic signals at a single junction. Transport. Res. Part B: Methodol. 22 (5), 357–370.
Hagen, L., Lin, P.-S., Fabregas, A.D., 2006. A Toolbox for Reducing Queues at Freeway Off-Ramps. University of South Florida, Tampa, Florida, USA.
He, Q., Kamineni, R., Zhang, Z., 2016. Traffic signal control with partial grade separation for oversaturated conditions. Transport. Res. Part C: Emerg. Technol. 71, 267–283.
Head, L., Gettman, D., Bullock, D.M., Urbanik, T., 2007. Modeling traffic signal operations with precedence graphs. Transport. Res. Rec.: J. Transport. Res. Board 2035, 10–18.
Jin, X., Cheu, R.L., Srinivasan, D., 2002. Development and adaptation of constructive probabilistic neural network in freeway incident detection. Transport. Res. Part C: Emerg. Technol. 10 (2), 121–147.
Lam, W.H., Poon, A.C., Mung, G.K., 1997. Integrated model for lane-use and signal-phase designs. J. Transport. Eng. 123 (2), 114–122.
Lee, S., Wong, S.C., Li, Y.C., 2015. Real-time estimation of lane-based queue lengths at isolated signalized junctions. Transport. Res. Part C: Emerg. Technol. 56, 1–17.
Li, Z., Chang, G.-L., Natarajan, S., 2009. Integrated off-ramp control model for freeway traffic management. In: Transportation Research Board 88th Annual Meeting, Washington, DC, pp. 1–12.
Lim, K., Ju, H.K., Shin, E., Kim, D.G., 2011. A signal control model integrating arterial intersections and freeway off-ramps. KSCE J. Civil Eng. 15 (2), 385–394.
Liu, Y., Chang, G.L., Yu, J., 2011. An integrated control model for freeway corridor under nonrecurrent congestion. IEEE Trans. Veh. Technol. 60 (4), 1404–1418.
Liu, Y., Li, P., Wehner, K., Yu, J., 2013. A generalized integrated corridor diversion control model for freeway incident management. Comp.-Aided Civil Infrastruct. Eng. 28 (8), 604–620.
Lu, J., Geng, N., Chen, H., 2010. Impacts of freeway exit ramp configurations on traffic operations and safety. Adv. Transport. Stud. 22, 5–16.
Ma, W., Head, K.L., Feng, Y., 2014. Integrated optimization of transit priority operation at isolated intersections: a person-capacity-based approach. Transport. Res. Part C: Emerg. Technol. 40 (1), 49–62.
Mahalel, J.H., David, 2014. Offset effects on the capacity of paired signalised intersections during oversaturated conditions. Transport. Transp. Sci. 10 (8), 740–758.
Mirchandani, P., Head, L., 2001. A real-time traffic signal control system: architecture, algorithms, and analysis. Transport. Res. Part C: Emerg. Technol. 9 (6), 415–432.
Muñoza, J.C., Laval, J.A., 2006. System optimum dynamic traffic assignment graphical solution method for a congested freeway and one destination. Transport. Res. Part B: Methodol. 40 (1), 1–15.
Munoz, J.C., Daganzo, C.F., 2002. The bottleneck mechanism of a freeway diverge. Transport. Res. Part A: Pol. Pract. 36 (6), 483–505.
Newell, G.F., 1999. Delays caused by a queue at a freeway exit ramp. Transport. Res. Part B: Methodol. 33 (5), 337–350.
Rudjanakanoknad, J., 2012. Capacity change mechanism of a diverge bottleneck. Transport. Res. Rec.: J. Transport. Res. Board 2278, 21–30.
Shen, W., Zhang, H.M., 2009. On the morning commute problem in a corridor network with multiple bottlenecks: its system-optimal traffic flow patterns and the realizing tolling scheme. Transport. Res. Part B: Methodol. 43 (3), 267–284.
Sheu, J.B., Yang, H., 2008. An integrated toll and ramp control methodology for dynamic freeway congestion management. Physica A 387 (16–17), 4327–4348.
Spiliopoulou, A., Kontorinaki, M., Papageorgiou, M., Kopelias, P., 2014. Macroscopic traffic flow model validation at congested freeway off-ramp areas. Transport. Res. Part C: Emerg. Technol. 41, 18–29.
Sun, W., Wu, X., Wang, Y., Yu, G., 2015. A continuous-flow-intersection-lite design and traffic control for oversaturated bottleneck intersections. Transport. Res. Part C: Emerg. Technol. 56, 18–33.
Tian, Z., Urbanik, T., Gibby, R., 2007. Application of diamond interchange control strategies at closely spaced intersections. Transport. Res. Rec.: J. Transport. Res. Board 2035, 32–39.
Tian, Z.Z., Kevin, B., Roelof, E., Larry, R., 2002. Integrated control strategies for surface street and freeway systems. Transport. Res. Rec.: J. Transport. Res. Board 1811, 92–99.
Tian, Z.Z., Wu, N., 2012. Probability of capacity enhancement and disruption for freeway ramp controls analysis by gap-acceptance and queuing models. Transport. Res. Rec.: J. Transport. Res. Board 2278, 1–12.
TRB, 2010. Highway Capacity Manual 2010. Transportation Research Board, Washington, DC.
Wong, C., Wong, S., 2002. Lane-based optimization of traffic equilibrium settings for area traffic control. J. Adv. Transport. 36 (3), 349–386.
Wong, C., Wong, S., 2003a. A lane-based optimization method for minimizing delay at isolated signal-controlled junctions. J. Math. Model. Alg. 2 (4), 379–406.
Wong, C., Wong, S., 2003b. Lane-based optimization of signal timings for isolated junctions. Transport. Res. Part B: Methodol. 37 (1), 63–84.
Wong, C.K., Heydecker, B., 2011. Optimal allocation of turns to lanes at an isolated signal-controlled junction. Transport. Res. Part B: Methodol. 45 (4), 667–681.
Wong, C.K., Wong, S.C., Tong, C.O., 2006. A lane-based optimization method for the multi-period analysis of isolated signal-controlled junctions. Transportmetrica 2 (1), 53–85.
Yan, C., Jiang, H., Xie, S., 2014. Capacity optimization of an isolated intersection under the phase swap sorting strategy. Transport. Res. Part B Methodol. 60 (1), 85–106.
Yang, X., Lu, Y., Chang, G.L., 2014. Dynamic signal priority control strategy to mitigate off-ramp queue spillback to freeway mainline segment. Transport. Res. Rec.: J. Transport. Res. Board 2438, 1–11.
Yang, X.F., Cheng, Y., Chang, G.L., 2015. A multi-path progression model for synchronization of arterial traffic signals. Transport. Res. Part C: Emerg. Technol. 53, 93–111.
Yi, Q., Chen, X., Li, D., 2012. Development of Warrants for Installation of Dual Right-Turn Lanes at Signalized Intersections. Southwest Region University Research Center, Texas, USA.
Zhao, J., Ma, W., Head, K.L., Yang, X., 2014a. Optimal intersection operation with median u-turn lane-based approach. Transport. Res. Rec.: J. Transport. Res. Board 2439, 71–82.
Zhao, J., Ma, W., Liu, Y., Yang, X., 2014b. Integrated design and operation of urban arterials with reversible lanes. Transport. B-Transp. Dyn. 2 (2), 130–150.
Zhao, J., Ma, W., Zhang, H.M., Yang, X., 2013. Increasing the capacity of signalized intersections with dynamic use of exit lanes for left-turn traffic. Transport. Res. Rec.: J. Transport. Res. Board 2355, 49–59.
Zhong, R.X., Sumalee, A., Pan, T.L., Lam, W.H.K., 2014. Optimal and robust strategies for freeway traffic management under demand and supply uncertainties: an overview and general theory. Transport. A: Transp. Sci. 10 (10), 849–877.